JTTEE5 12:53-69

A Stochastic Model to Simulate the Formation of a Thermal Spray Coating

R. Ghafouri-Azar, J. Mostaghimi, S. Chandra, and M. Charmchi

(Submitted 28 September 2001; in revised form 17 January 2002)

We present a three-dimensional, stochastic model of thermal spray coating. It is capable of predicting coating porosity, thickness, roughness, and the variation of these properties with spray parameters. The model assigns impact properties to molten droplets landing on the substrate by generating random values of process parameters, assuming that these properties follow normal distributions with user-specified means and standard deviations. We prescribed rules to calculate splat sizes after droplet impact and their interaction with each other. Porosity is assumed to be solely due to the curl-up of the splats as a result of thermal stresses. We use a Cartesian grid to define the computational domain and to track the shape and position of the deposited coating. The surface of the coating and the location of pores within it are specified using a variable known as the "volume fraction," defined as the fraction of the volume of a computational cell occupied by coating material. Results are given for the variation of coating porosity, thickness and roughness with varying particle speed, size, and spraying gun speed. Predicted trends agree with experimental observation.

Keywords coating formation, deposition, microstructure, simulation, stochastic

1. Introduction

Thermal spray coating is a relatively mature technology widely used in industry. But, despite the extensive literature published on processes such as plasma spraying or high-velocity oxyfuel (HVOF) spraying, thermal spray coating still remains as much an art as a science. The user has to select suitable values for a large number of variables, including the power of the torch, gas flow rates, substrate standoff distance, powder feed rate, and speed of torch movement. Coating quality depends a great deal on the skill of the operator in selecting these parameters, which differ for each coating material. Typically a lengthy process of trial-and-error goes into optimizing thermal spray operations for any given application.[1] Since the equipment is expensive to operate, the cost of developing new coatings can be very high.

A computer model capable of predicting coating properties as a function of process parameters could, in principle, greatly reduce development time. However, the physical mechanism by which a thermal spray coating is formed is so complex that few attempts have been made to simulate it. Figure 1 shows a schematic view of the thermal spray coating process. Fine particles are fed into a hot carrier gas where they melt while being propelled at high velocity onto the surface to be coated. Molten droplets land on the solid surface where they spread, solidify, and agglomerate to form a thin layer.

Inspection of a cross section through a thermal spray coating (see Fig. 2) shows that it is built up of thin lamellae formed by flattened droplets that land on each other and fuse together. Closer examination shows that the coating is not fully dense: pores are found at the interface between splats.[2-4] The presence of these pores may or may not be desirable, depending on the purpose of the coating. Porosity is detrimental to the performance of wear resistant coatings since it reduces their structural integrity and adhesion strength. But closed pores are useful in thermal barrier coatings since they reduce thermal conductivity and enhance insulation. In either case it is important to be able to produce the desired level of porosity by controlling the coating deposition process.

Knotek and Elsing[5] developed a model of thermal spray deposition that they used to predict the size and distribution of interlamellar cracks and pores in the coating. Their simulation used the Monte Carlo method in which particles with randomly varying diameter and velocity were deposited on a surface. The size of lamellae and pores formed by impacting droplets were determined according to simple guidelines, and the overall coating structure was determined. The model was two-dimensional, so that it predicted only the structure of a single cross section through the deposited layer.

Cirolini et al.[6,7] also simulated coating deposition with a two-dimensional stochastic model and postulated a much more complex set of rules to represent interactions between splats landing on each other. Kanouff et al.[8] modeled coating by a thermal spray inclined at an angle to the substrate and calculated the surface roughness of the coating. Hansbo and Nylen[9] developed a model to simulate layer build-up and robot motion without any attention to the internal coating microstructure.

Though the literature on modeling deposition of entire sprays is relatively sparse, a great deal more has been published on the impact and solidification of a single molten droplet on a solid surface. Madejski[10] developed a simple analytical model to estimate the maximum spreading diameter of alumina splats. Zhao et al.[11,12] used both experiments and a two-dimensional numerical model to study fluid dynamics and heat transfer during the impact of liquid droplets on a solid substrate. Pasandideh-

R. Ghafouri-Azar, J. Mostaghimi, and **S. Chandra,** Department of Mechanical and Industrial Engineering, University of Toronto, Toronto, Ontario, Canada; and **M. Charmchi,** Department of Mechanical Engineering, University of Massachusetts, Lowell, MA. Contact e-mail: rezaa@mie.utoronto.ca.

Fard et al.[13] simulated the axisymmetric impact and solidification of tin droplets on a steel plate and validated the model with experiments. Bussmann et al.[14] developed a three-dimensional model of liquid droplet impact that could be used to simulate droplets impinging on a surface of arbitrary shape. Pasandideh-Fard et al.[15] extended Bussmann et al.'s code by including solidification. A number of experimental investigations[16-20] into the impact of individual molten droplets on a solid surface have examined the effect of varying parameters such as impact velocity, substrate temperature, and droplet size on droplet spreading and splashing.

Two-dimensional models of thermal spray coating are of only limited use in predicting thermal spray coating structures, since the process is inherently three-dimensional. Pores and cracks form a network within the deposited layer, and a single cross section through it gives incomplete information. If the substrate has a complex shape, rather than being flat, the coating structure may change significantly with location.

The objective of the study described in this paper was to develop a three-dimensional stochastic model of thermal spray coating capable of predicting coating porosity, thickness and roughness, and the variation of these properties with spray parameters. The model dispersed molten droplets on the substrate by generating random values of process parameters, assuming that these properties follow appropriate distributions with user-specified means and standard deviations. Splat sizes after droplet impact were calculated from an analytical model.[19] We used a deliberately simple set of rules to describe coalescence of splats. Porosity was assumed to be solely due to the curl-up of the splats as a result of thermal stresses. We will demonstrate that even such an idealized description of interactions between splats can be used to generate fairly realistic coating properties. In the future, we plan to use a three-dimensional model of droplet impact and splashing[15] to generate more sophisticated rules for predicting splat shapes, and to determine what is the least level of complexity required for these rules to predict values of porosity and thickness that agree well with experimental results.

2. Numerical Method

2.1 Process Parameters

Physical properties of coatings produced by thermal spray have been found to be sensitive to a large number of process parameters such as droplet size distribution, velocity, temperature, and substrate properties at the point of impact. Measurement of these parameters for every particle in a spray is prohibitively difficult, but their statistical distributions can be easily

Nomenclature

C	specific heat
d	diameter of splat
D	diameter of droplet
f	volume fraction
F	cumulative probability
g	probability density function
h	thickness
H_f	latent heat of fusion
l	distance between center point of splats
L	substrate length
N	number of cells
P	porosity
$p(x,y)$	splat boundary profile
R_a	average surface roughness
S	random variant
t	time
t_c	time of spreading
t	temperature
U	gun speed
V	particle speed
W	substrate width
X	cell location with respect to splat center point
Z	gun distance from substrate

Subscripts, Superscripts

c	coating
cell	cell
g	gap
gun	gun
i	discretized x-direction
j	discretized y-direction
k	discretized z-direction
l	log-population
m	average amount of values
mat	material
max	maximum
n	number of splat
q	previously deposited splat counter (q = 1,…,n-1)
sub	substrate
sp	splat
x	x direction
y	y direction

Greek Symbols

α	curl up angle of splat
δ	liquid-solid contact angle
Γ	process parameter
γ	surface tension
η	dummy variable
λ	thermal diffusivity
μ	mean value of probability density function
ν	kinematic viscosity
θ	azimuthal angle
ρ	density
σ	standard deviation of probability density function
ξ	spread factor
ω	disperse angle

Dimensionless Numbers

Pe	Peclet number (Pe = VD/λ)
Re	Reynolds number (Re = VD/ν)
Ste	Stefan number (Ste = $C(T-T_{sub})/H_f$)
We	Weber number (We = $\rho V^2 D/\gamma$)

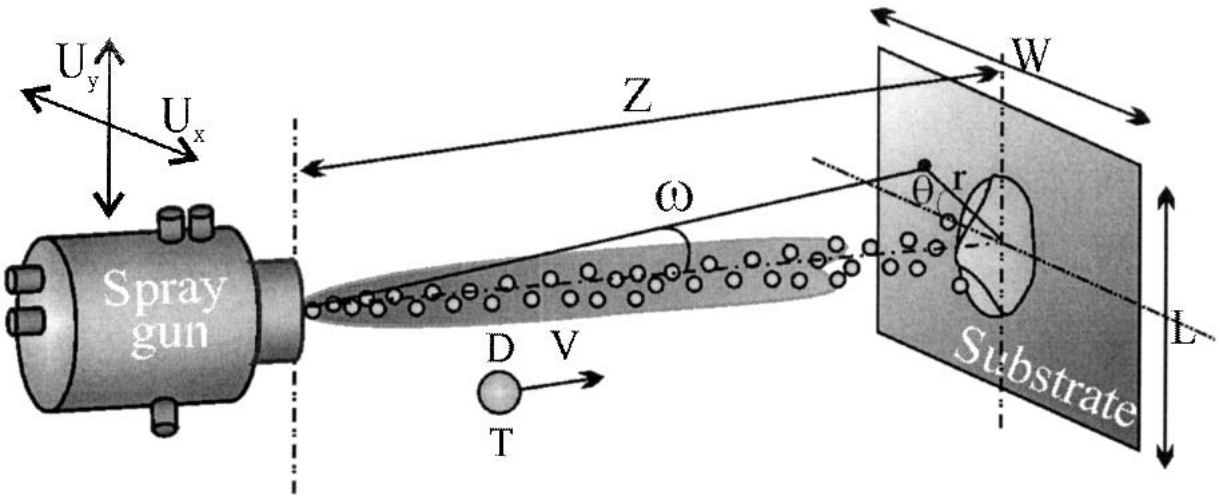

Fig. 1 Schematic diagram of a thermal spray process

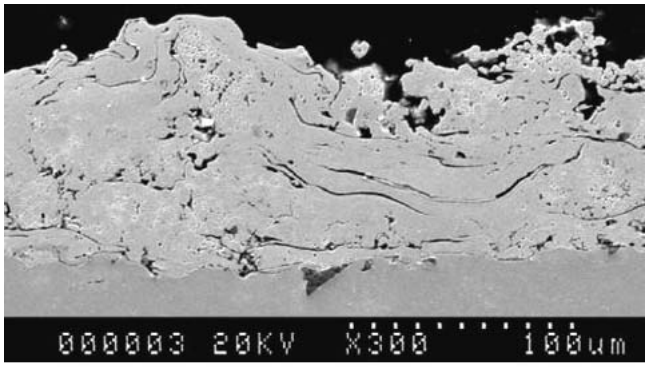

(a)

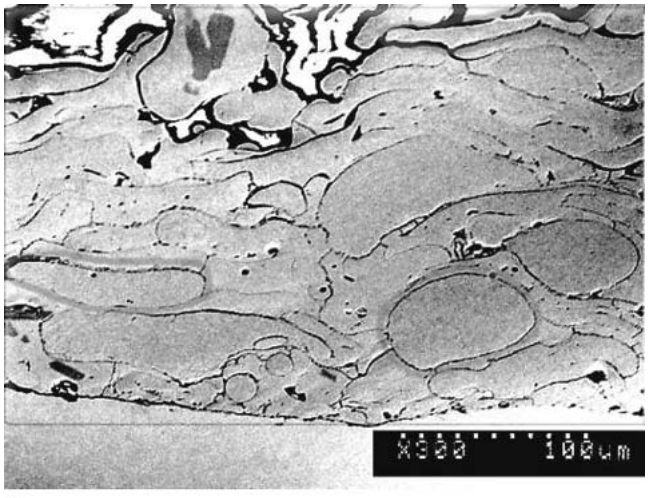

(b)

Fig. 2 Scanning electron microscope (SEM) micrograph of thermal spray coating microstructure **(a)** nickel plasma sprayed on stainless steel with V = 62 m/s, T = 1570 °C, D = 43µm, porosity = 7.7%; **(b)** closer view of cross section through coating, showing lamellar microstructure

determined experimentally using commercially available instruments. For example, the DPV-2000 monitoring system from Tecnar Ltd. (Montreal, Canada) simultaneously measures diameter, velocity, and temperature of particles in a thermal spray and calculates their statistical distribution. In our stochastic model of coating formation, we assumed that the particle speed V, diameter D, temperature T, and impact point (defined by ω and θ, the two angles shown in Fig. 1) have random, continuously varying values. Measurements of particle properties in thermal sprays performed by DPV-2000[21,22] have shown that the variation of velocity and temperature can be represented reasonably well by a normal probability distribution (Fig. 3) denoted by $N(\mu,\sigma^2)$ with probability density function (PDF) given by:

$$g(x) = \frac{1}{\sigma\sqrt{2\pi}}\exp\left(-\frac{1}{2\sigma^2}(x-\mu)^2\right) \quad \text{(Eq 1)}$$

where g represents any distributed variable, μ the mean value, and σ the standard deviation.

Particle size distributions are better described[23] by a lognormal PDF ($LN(\mu,\sigma^2)$) defined as:

$$g_l(x) = \frac{1}{x\sigma_l\sqrt{2\pi}}\exp\left(-\frac{1}{2\sigma_l^2}(\ln x-\mu_l)^2\right) \quad \text{(Eq 2)}$$

where μ_l is the log-population mean and σ_l is the log-population standard deviation. Figure 3 shows measurements of size, velocity, and temperature of nickel particles in a plasma spray made by using a DPV 2000 system. Next to the experimental measurements are distributions of the same properties generated by the model using experimentally measured mean values and standard deviations.

We used a spherical coordinates system to define the landing positions of particles, characterized by the distance of the gun from the substrate (Z), disperse angle (ω), and azimuthal angle (θ). For each particle, ω was assumed to follow a normal distribution, with its mean along the axis of the spray gun, while all

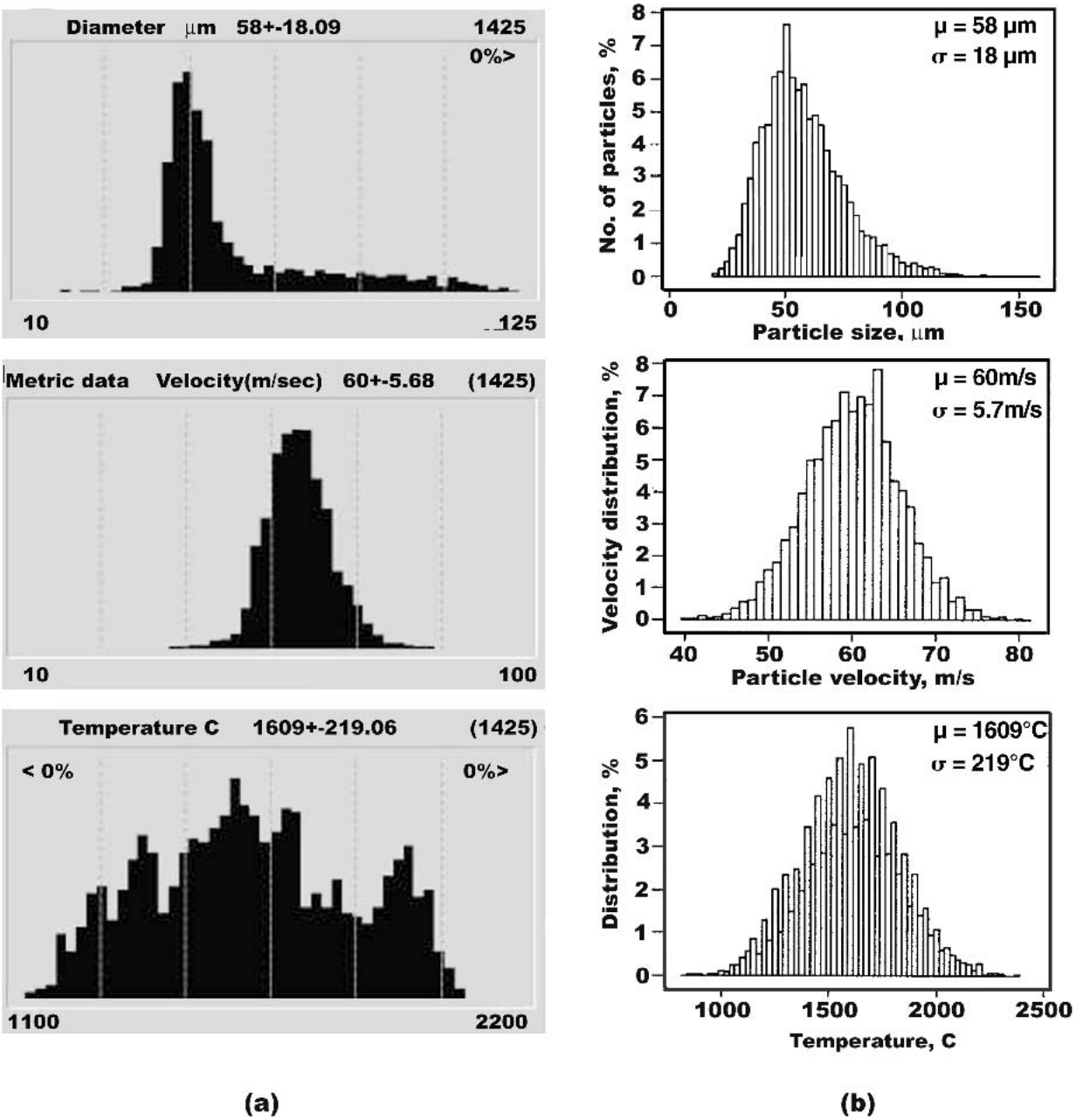

Fig. 3 **(a)** Typical measurements of particle size, velocity, and temperature distributions of nickel particles in a plasma spray made with a DPV-2000 monitoring system from Tecnar (Montreal, Canada); **(b)** distributions of particle size, velocity, and temperature generated by the model

values of θ were considered equally probable. The impact coordinates were calculated from:

$$\begin{cases} x_c = Z \tan(\omega) \cos(\theta) \\ y_c = Z \tan(\omega) \sin(\theta) \end{cases} \quad \text{(Eq 3)}$$

The procedure for calculating random values of process parameters with a normal distribution was as follows[24]:

1) Guess a uniformly distributed random number U between (0,1).
2) Calculate the random variate S that has the cumulative probability distribution function $F(x)$ by $S = F^{-1}(U)$.
3) Evaluate the required parameter Γ using specified values of the mean and standard deviation and the calculated S: $\Gamma = \mu_\Gamma + S\sigma_\Gamma$.

To generate values of particle diameters, which followed a log-normal distribution, we calculated Γ_1 using the procedure described above, and then took $\Gamma = e^{\Gamma_1}$ as the value to be used.

2.2 Splat Shapes

Having assigned a velocity, size, and temperature to each droplet in the spray, we can calculate the size of the splat formed by it after impacting on a solid surface using a simple analytical expression proposed by Aziz and Chandra.[19] The model assumes that the spherical droplet spreads to form a cylindrical disc of diameter d_{max} and thickness h_s, and neglects the effects of any droplet splashing and break-up. The maximum splat diameter (d_{max}) is nondimensionalized by the initial droplet diameter (D) to give the maximum spread factor ($\xi_{max} = d_{max}/D$). An energy balance[19] shows that ξ_{max} is a function of the Weber number ($We = \rho V^2/\gamma$), Reynolds number ($Re = VD/\nu$), Stefan number ($Ste = C(T-T_{sub})/H_f$), Peclet number ($Pe = VD/\lambda$), and liquid-solid contact angle δ:

$$\xi_{max} = \sqrt{\frac{We + 12}{3(1 - \cos\delta) + 4\frac{We}{\sqrt{Re}} + We\sqrt{(3St)/(4Pe)}}} \quad \text{(Eq 4)}$$

We estimated the diameter of a splat formed by the impact and solidification of a molten droplet from the above equation. For thermal spray conditions, the magnitude of the term containing δ is very small compared with the other terms in the denominator,[19] and it was neglected. The thickness of the splat was calculated by equating the volume of a droplet of diameter D to a cylinder of diameter d_{max} and thickness h_s, so that $h_s = (2D)/(3\xi_{max}^2)$.

When a superheated droplet lands on a previously deposited splat, material at the interface between them melts and the two fuse together. The shape of the combined splat depends on the distance between the centers of the two splats. Shakeri[25] did a series of experiments in which 2.2 mm molten tin droplets were dropped sequentially onto a stainless steel plate, with the second droplet deposited at a small offset from the center of the first. Figure 4 shows the different splat shapes that were obtained for different offset distances. The splat shapes closely resembled those observed in experiments where a steel substrate was rapidly passed through a plasma jet in which nickel particles were being sprayed, so that a few splats collected on the surface. Figure 5(a) shows two nickel droplets, each approximately 70 μm in diameter, deposited such that their edges overlap. Their shape closely resembles that of the 2.2 mm tin droplets (Fig. 5b).

Based on these experimental results, and some simulations of sequential droplet impact using a three-dimensional model,[26] we developed four possible scenarios as to the splat shape formed by droplet interactions (Fig. 6). To select one of these splat shapes after a particle was deposited, the distances between the droplet impact point and the center point of all previously deposited splats was evaluated. The smallest value of these distances gave the distance (l) to the closest deposited splat, that is:

$$l = \text{Min}(|l_n|), \qquad n = 1,2,3, \ldots . \quad \text{(Eq 5)}$$

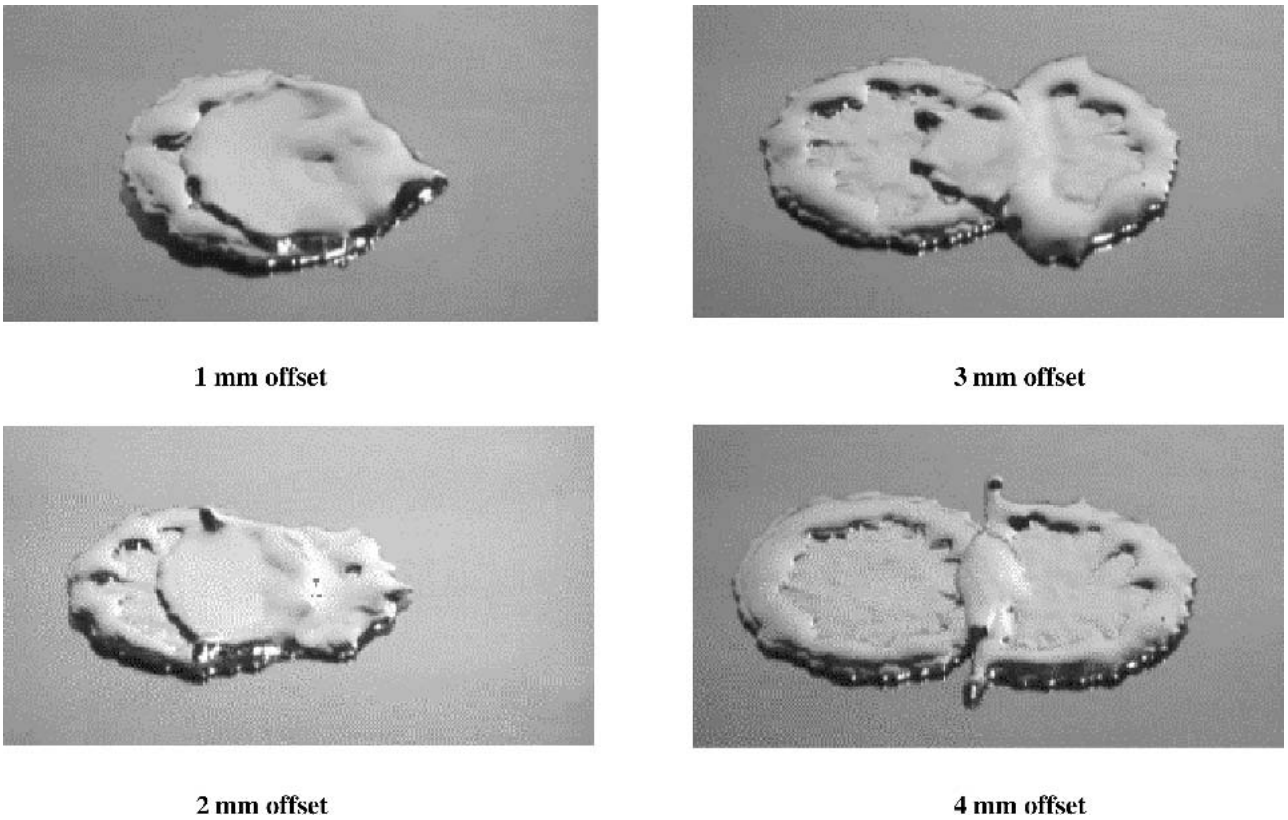

Fig. 4 Splats formed by deposition of two 2.2 mm diameter tin droplets with an impact speed of 2.5 m/s on a stainless steel plate, with the center of the second drop offset from the first

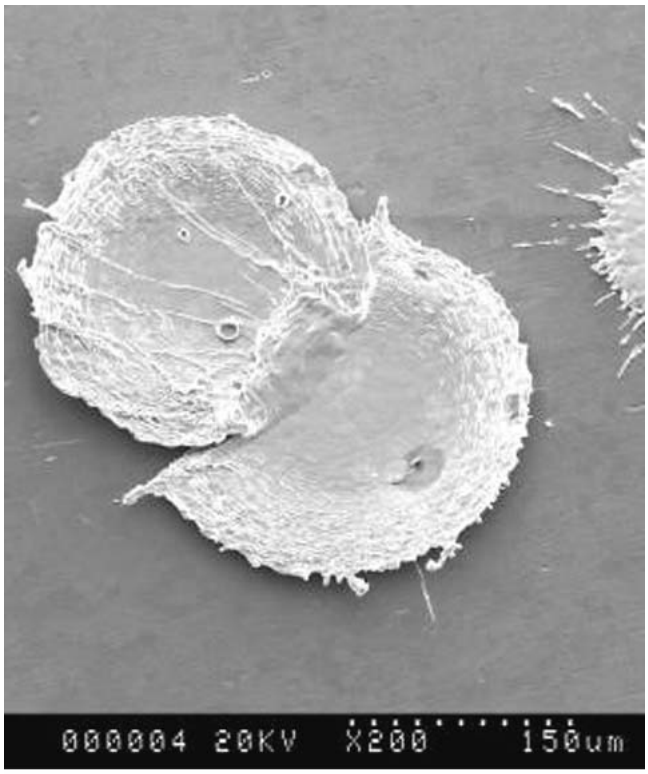

(a)

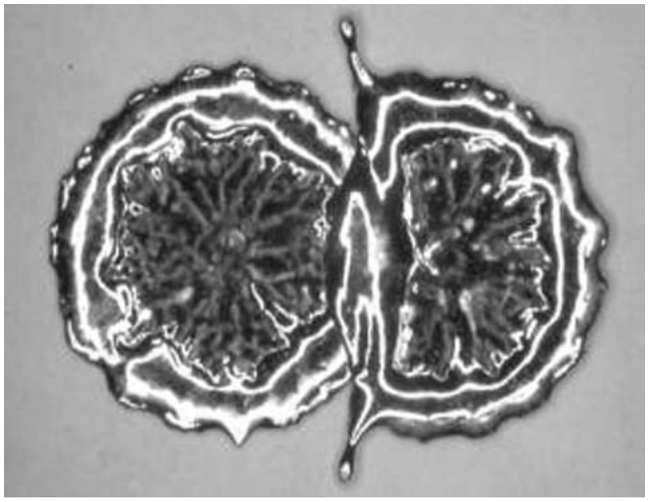

(b)

Fig. 5 Splats formed by deposition of **(a)** two nickel droplets sprayed from a plasma torch onto a stainless steel surface; **(b)** two 2.2. mm diameter tin droplets dropped with an impact speed of 2.5 m/s on a stainless steel plate, with the center of the second drop offset by 44 mm from the first

where

$$l_n = (x_{c,n} - x_{c,q})\hat{i} + (y_{c,n} - y_{c,q})\hat{j} \qquad q = 1,2,3\ldots n-1 \quad \text{(Eq 6)}$$

$x_{c,n}$ and $y_{c,n}$ in the equation indicate the coordinates of the center of the impacting droplet. Splat shapes were selected using the following set of rules:

$$\begin{cases} 0 \le l < \dfrac{7D_m}{8} & \text{Splat No. 1} \\ \dfrac{7D_m}{8} \le l < D_m & \text{Splat No. 2} \\ D_m < l \le \dfrac{9D_m}{8} & \text{Splat No. 3} \\ \dfrac{9D_m}{8} < l \le \dfrac{D_n + D_m}{2} & \text{Splat No. 4} \end{cases} \quad \text{(Eq 7)}$$

For the case where $l > (D_n + D_m)/2$, there is no overlap between splats. Here, D_n is the diameter of the splat formed by the droplet under consideration, and D_m is the diameter of the nearest previously deposited splat. For circular disc-shaped splats, the analytical spread factor relation (Eq 4) was applied to calculate the splat diameter. In the case of noncircular splats, the shape was selected using Eq 7, and the splat area A_n was assumed to be the same as that given for a circular splat by Eq 4.

2.3 Formation of Pores

A coating consists of both solid material with volume V_m and voids with volume V_g. Porosity (p) is defined as the fraction of the total coating volume ($V_g + V_m$) occupied by voids so that:

$$p = \frac{V_g}{V_g + V_m} \quad \text{(Eq 8)}$$

Several possible sources of porosity in a coating have been identified including: curling up of splats due to thermal stresses[6,7]; incomplete filling of interstices during deposition[3,27]; presence of unmelted particles in the spray[4]; satellite droplets formed by splat break-up at the time of impact; overshooting of liquid over solidified splats during droplet spreading; entrapment of gas between splats[3,28]; and the presence of oxide layer on the spray particles.[4] Figures 7 and 8 show micrographs of nickel splats deposited on a stainless steel surface using a plasma torch. The various phenomena listed above are visible in these images, including splashing of droplets and unmelted particles (Fig. 7). A cross section through a splat (Fig. 8) clearly shows the curvature of the splat due to thermal stresses: pores form under the elevated edges of the splat. In this study, we assumed that this last effect, splat curvature, was the only mechanism creating porosity. Based on experimental evidence, splats were assumed to detach from the substrate starting at a distance $0.6R$ from the center,[28] where R is the splat radius (Fig. 9). The angle of detachment was defined as $\alpha = \tan^{-1}(h_{g,R}/(0.4R))$, where $h_{g,R}$ was the gap thickness at the edge of the splat (Fig. 9). α was assumed to be randomly distributed along a normal distribution (Eq 1), whose mean and standard deviation were supplied as inputs to the model.

2.4 Coating Build-Up

We used a three-dimensional Cartesian grid to define the computational domain and to track the shape and position of the coating surface. The x and y coordinates lay in the plane of the substrate and the z axis was perpendicular to it. The structure of the coating was defined using a variable known as the "volume

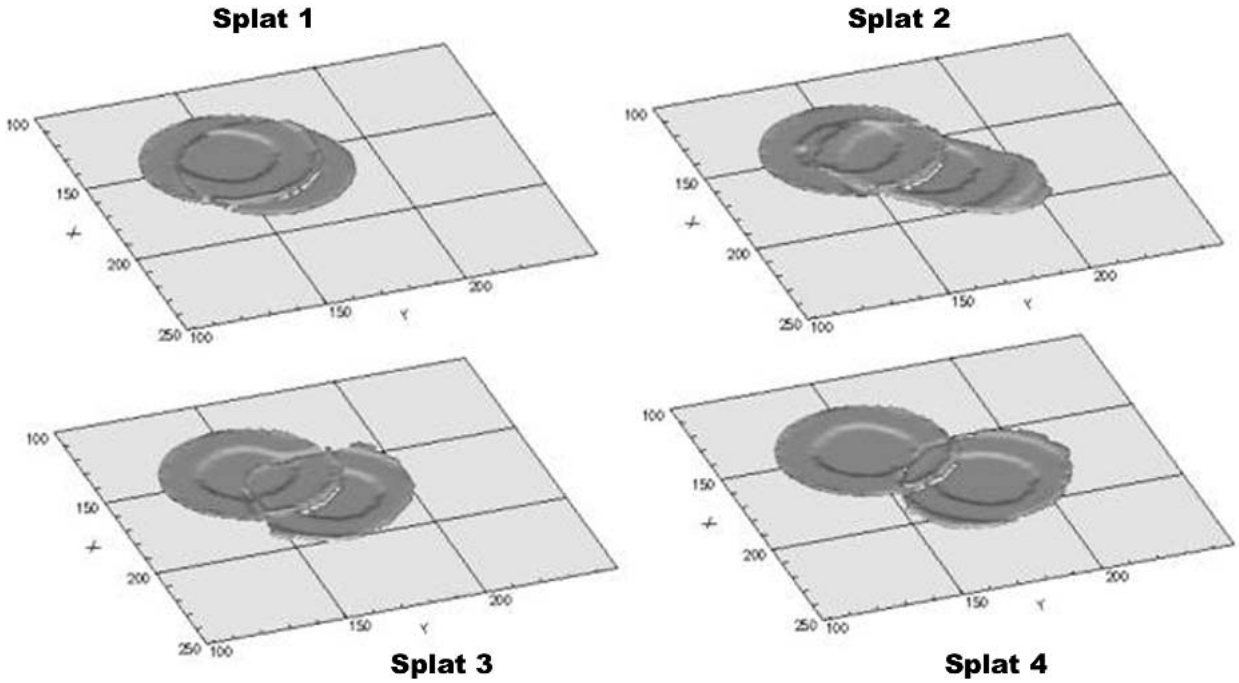

Fig. 6 Assumed splat shapes for the deposition of one nickel droplet on top of the other, for varying center offset distances

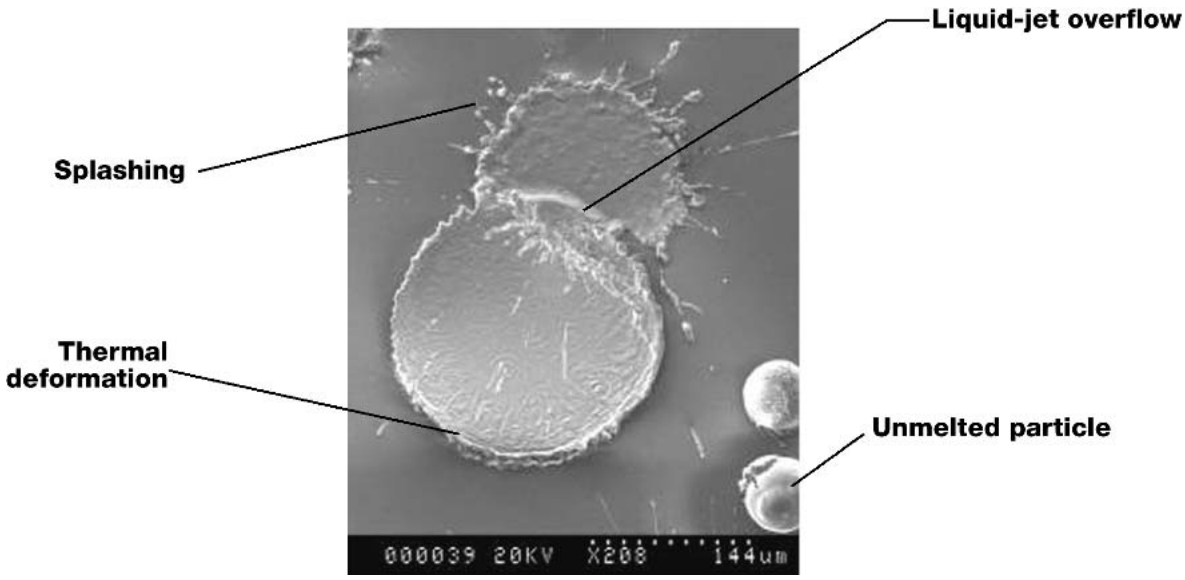

Fig. 7 Nickel particles deposited by plasma spray on a glass substrate

fraction" (f), defined as the fraction of the cell volume V_{cell}, occupied by coating material (V_{mat}), so that:

$$f_{i,j,k} = \frac{V_{mat}}{V_{cell}} \quad \text{(Eq 9)}$$

or

$$f_{i,j,k} = \frac{1}{\Delta x_i \Delta y_j \Delta z_k} \int_{\Delta x_i} \int_{\Delta y_j} \int_{\Delta z_k} f_s \, dz dy dx \quad \text{(Eq 10)}$$

where

$$f_s = \begin{cases} 1 & \text{inside the splat} \\ 0 & \text{outside of splat} \end{cases} \quad \text{(Eq 11)}$$

Hence, $f_{i,j,k}$ equals unity when the cell is filled with material and zero when the cell is empty. For a partially filled cell, $0 < f_{i,j,k} < 1$, as may be the case when the cell is at the coating boundary or contains a pore. Figure 10 illustrates partially filled cells near the edge of a splat.

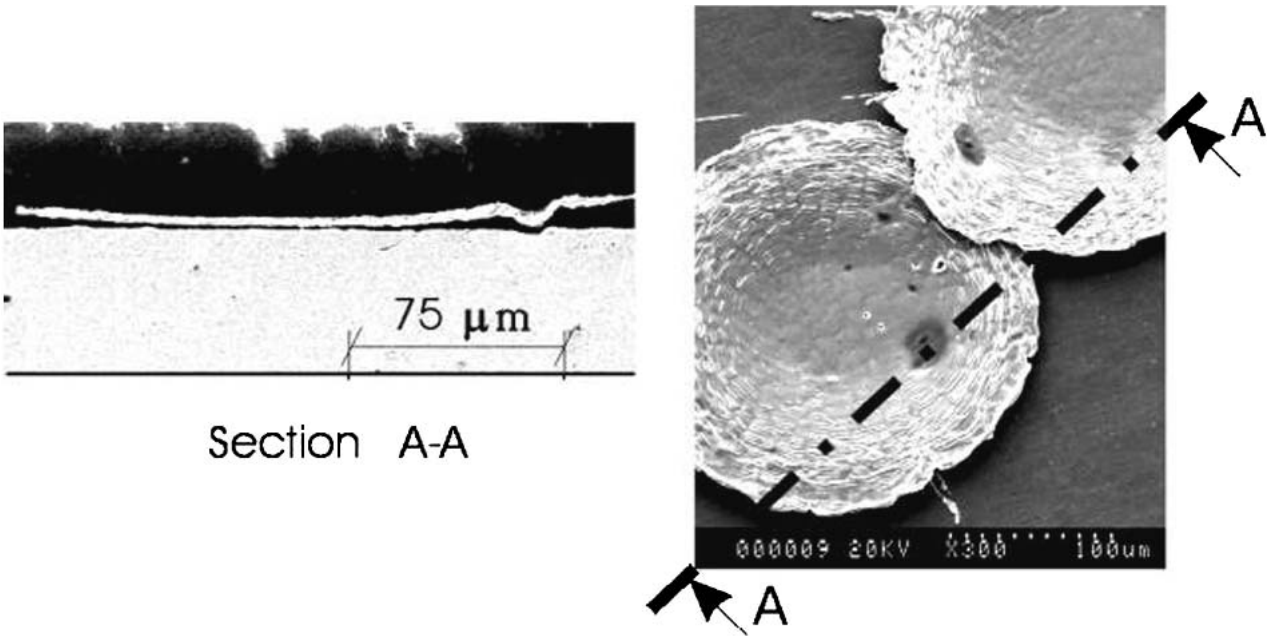

Fig. 8 Top view and cross section through nickel particles deposited by plasma spray on a stainless steel substrate. Curvature of splats due to thermal stresses can be seen.

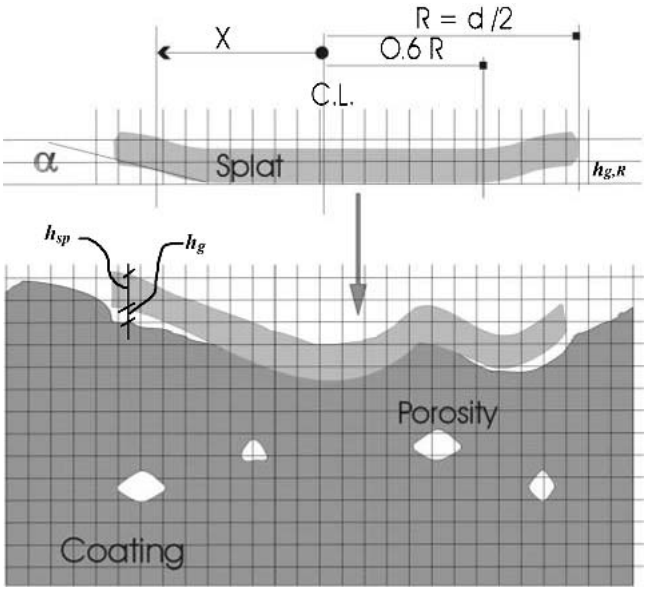

Fig. 9 Curl-up of splats after impact. Splats were assumed to detach from the substrate, starting at a distance $0.6R$ from the center, with an angle α.

A splat was generated in the model from a droplet whose volume, temperature, and location were specified by the stochastic model. Knowing the impact conditions, the splat area and shape were calculated from Eq 4 and 7. The splat area was defined in the computational grid by computing the fraction of splat area occupying the cell at coordinates *(i,j)* using

$$f_{i,j} = \frac{1}{\Delta x_i \Delta y_j} \int_{\Delta x_i} \int_{\Delta y_j} f_s \, dy dx \qquad \text{(Eq 12)}$$

Figure 11 illustrates how two different splat shapes were discretized. Along boundary cells, the computational mesh was further subdivided to improve resolution of the splat edges. A three-dimensional splat was created by projecting the splat area in a direction perpendicular to the substrate through a distance sufficient to make the splat volume equal to that of the droplet before impact. The splat thickness was assumed to be uniform.

Figure 9 illustrates how a splat was transformed when it was deposited onto the irregular surface of the coating. The shape of the splat was modified to conform to the surface under it, while keeping its thickness the same, and the splat material was added to that of the existing coating. It was assumed that the splat completely filled all cavities under it in the region $0 \le X_{i,j} < 0.6R$, where there was no curl-up. Under the curled up edges of the splat (for $0.6R \le X_{i,j} \le R$), the voids under the deposited splat were preserved intact, by keeping h_g constant, when the splat was deposited on the existing coating.

Coating build-up is a result of splat agglomeration with pores, if any, being trapped between impacting splats and the pre-existing coating. Therefore, the increase in coating thickness ($h_c(x,y)$) during a given time interval (δt) is the sum of the splat thickness ($h_{sp}(x,y)$) and the gap between splats ($h_g(x,y)$), so that:

$$\frac{\delta h_c(x,y)}{\delta t}\Big|_{n-1\to n} = \frac{h_c^n(x,y) - h_c^{n-1}(x,y)}{\delta t}$$

$$= \begin{cases} h_{sp}^n(x,y) + h_g^n(x,y) & 0 < f_{i,j} \le 1 \\ 0 & f_{i,j} = 0 \end{cases} \qquad \text{(Eq 13)}$$

The superscripts n and n-1 refer to the current and previous time levels, respectively. The void fraction *f* throughout the coating

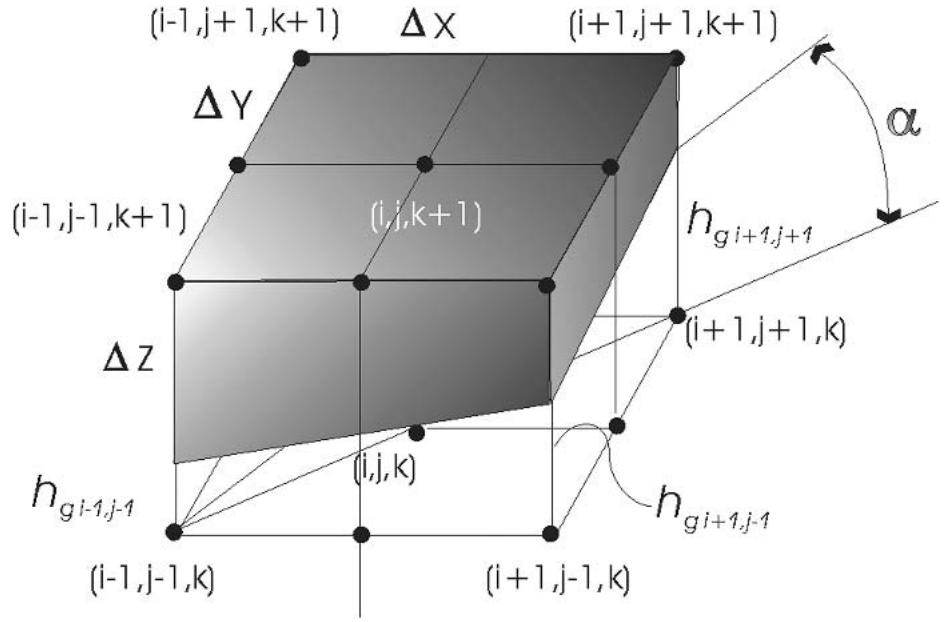

Fig. 10 Discretization of the edge of a splat

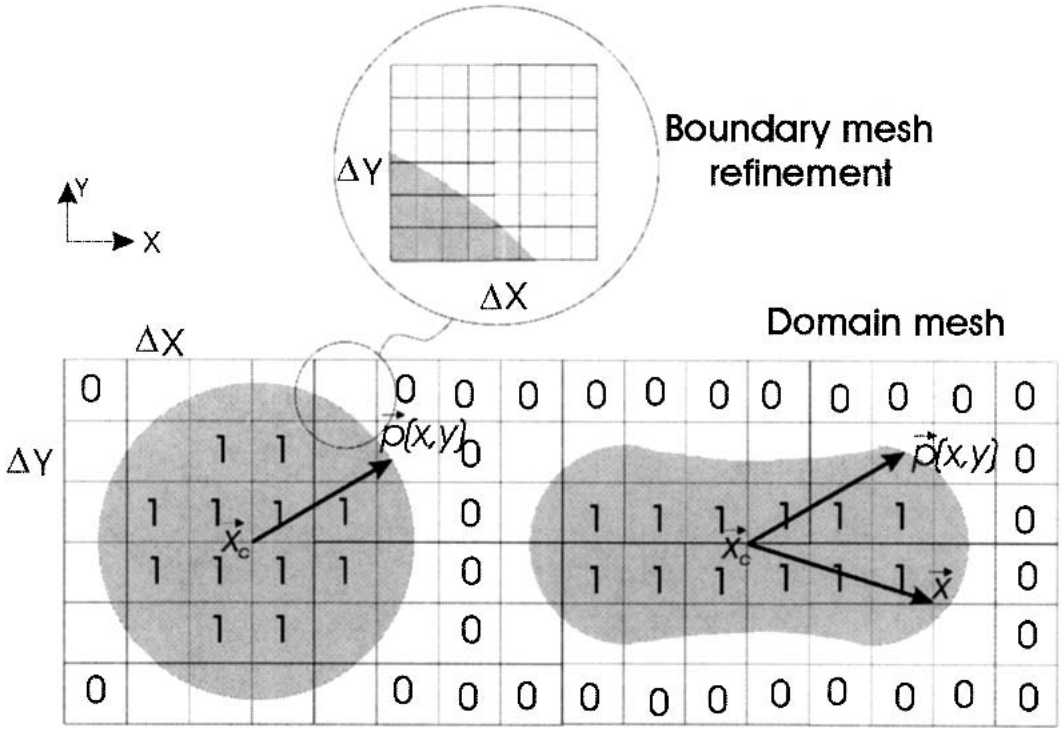

Fig. 11 Discretization of two different splat shapes in the computational mesh

was updated after each droplet was deposited, to keep track of the position of the coating surface and the location of pores.

Properties of coatings that are usually important in applications, and can be easily measured, include porosity (p), average thickness ($h_{c,m}$), and average surface roughness (R_a). We calculated each of these properties for the simulated coatings generated by the computer model. Porosity was calculated using:

$$p = 1 - \frac{\sum_{i,j,k} \rho f_{i,j,k} \Delta x_i \Delta y_j \Delta z_k}{\sum_{i,j,k} \Delta x_i \Delta y_j \Delta z_k} \qquad \text{(Eq 14)}$$

The average thickness of coating was defined as:

$$h_{c,m} = \frac{1}{N_L N_W} \sum_{i,j} h_c(x_i, y_j) \quad \text{(Eq 15)}$$

where N_L and N_W represent the number of grid points along the length and width of the substrate, respectively. The average coating roughness over a length l was estimated from:

$$R_a = \frac{1}{l} \int_0^l | h_c - h_{c,m} | dx \quad \text{(Eq 16)}$$

2.5 Gun Movement

In a typical thermal spray process, the spray gun moves continuously. To account for this in the model, the position of a droplet (x_c) was defined in a frame of reference that moved with the gun. The position of a droplet (x) relative to the substrate was given by:

$$x = x_{gun} + x_c \quad \text{(Eq 17)}$$

where x_{gun} denoted the gun position and was a function of time. The spray gun could be programmed to have any arbitrary user-defined velocity. For gun movement with constant velocity, the x-component of gun position over a substrate with dimensions of $L \times W$ were described by:

$$x_{gun} = \begin{cases} U_x \left(t - 2k \dfrac{L}{U_x} \right) & 2k \dfrac{L}{U_x} \le t < (2k+1) \dfrac{L}{U_x} \\ L - U_x \left(t - (2k+1) \dfrac{L}{U_x} \right) & (2k+1) \dfrac{L}{U_x} \le t < (2k+2) \dfrac{L}{U_x} \end{cases}$$

$$k = 0, 1, 2, \ldots \quad \text{(Eq 18)}$$

Here, t indicates the time measured from the start of spraying, U the gun velocity, and k an index indicating the number of passes (where a pass consists of both the forward and backward traverse) that the gun made over the substrate. Similarly, equations were written for the y-coordinate. The profile of a gun moving with sinusoidally varying velocity over the substrate, with maximum speed U_0, was given by

$$x_{gun} = \frac{L}{2} \left(1 - \cos\left(\frac{2 U_{0x}}{L} t \right) \right) \hat{i} + \frac{W}{2} \left(1 - \cos\left(\frac{2 U_{oy}}{W} \left(t - \frac{k\pi L}{2U_{0x}} \right) \right) \right) \hat{j} \quad \text{(Eq 19)}$$

The time taken t_c for each droplet to spread to its maximum extent is approximately[14]:

$$t_c = \frac{8D}{3V} \quad \text{(Eq 20)}$$

We calculated the average time ($\overline{\delta t}$) between deposition of two particles by dividing the average mass of a droplet by the mass flow rate of powder through the gun ($\dot{m}_{gun}$):

$$\overline{\delta t} = \frac{\rho \pi \overline{D}^3}{6 \dot{m}_{gun}} \quad \text{(Eq 21)}$$

Since the time required for a droplet to spread and solidify is much less than the average time between deposition of two particles, it was assumed that they impact on the substrate sequentially and that no two land at the same time.

3. Results of Simulations

We present results from simulations of the deposition of nickel particles on a stainless steel surface with both stationary and moving guns. Simulations were carried out using a mesh that had uniform grid spacing in the x and y directions (parallel to the substrate). The grid size in the z-direction was different in each case, selected as being half the average thickness of a splat ($\Delta z_k = \overline{h}/2$). Boundary cells along the edges of splats were further subdivided by a factor of 50 to improve resolution.

Mean values and standard deviations of particle velocities, temperatures, and diameters were based on typical measurements made from nickel particles in a plasma spray (Fig. 3). Based on experimental data, we selected values for the distributions of the angles ω and θ that defined the landing position of particles, and of α, the curl-up angle of the splat edges. The values of input parameters to the model are summarized in Table 1. Figure 12 illustrates typical random distributions of these parameters generated by the model.

The first set of results is from a simulation in which a gun was held stationary at a distance of 150 mm from the substrate, with a powder mass flow rate of 0.126 g/s; all other parameters are listed in Table 1. To keep the size of the computational data stored at a manageable level, only the coating deposited on a 1 mm × 1 mm area centered along the gun axis was modeled.

Figure 13(a) shows the predicted coating shape after 2 mg of powder was fed into the gun, which required 0.016 s of spraying time. Only 38.7% of the total mass sprayed from the gun landed on the 1 mm × 1 mm area considered in the computation. The simulation was performed on a grid with 252 points in both x and y directions ($\Delta x = \Delta y = 4$ μm) and 220 points in the z direction ($\Delta z = 2.5$ μm). As expected, the surface of the deposit follows a Gaussian distribution, with its thickness maximum at the center of the deposit and decreasing with distance from this point (see Fig. 13a). The shape is very similar to those observed in the experiments: Fig. 13(b) shows a nickel deposit formed by plasma spraying with the gun held

Table 1 Mean Values and Standard Deviations of Process Parameters

Particles Parameters	Mean Value, μ	Standard Deviation, σ
Velocity V [m/s]	60	5.7
Disperse angle ω [degrees]	0	0.5
Azimuthal angle θ [degrees] (uniform distribution)	0	0
Particle diameter D [μm] (log-normal)	58 (4.014)	18 (0.303)
Particle temperature T [K]	1609	219
Edge curl-up angle α [radians]	5h/(2d)	5h/(12d)

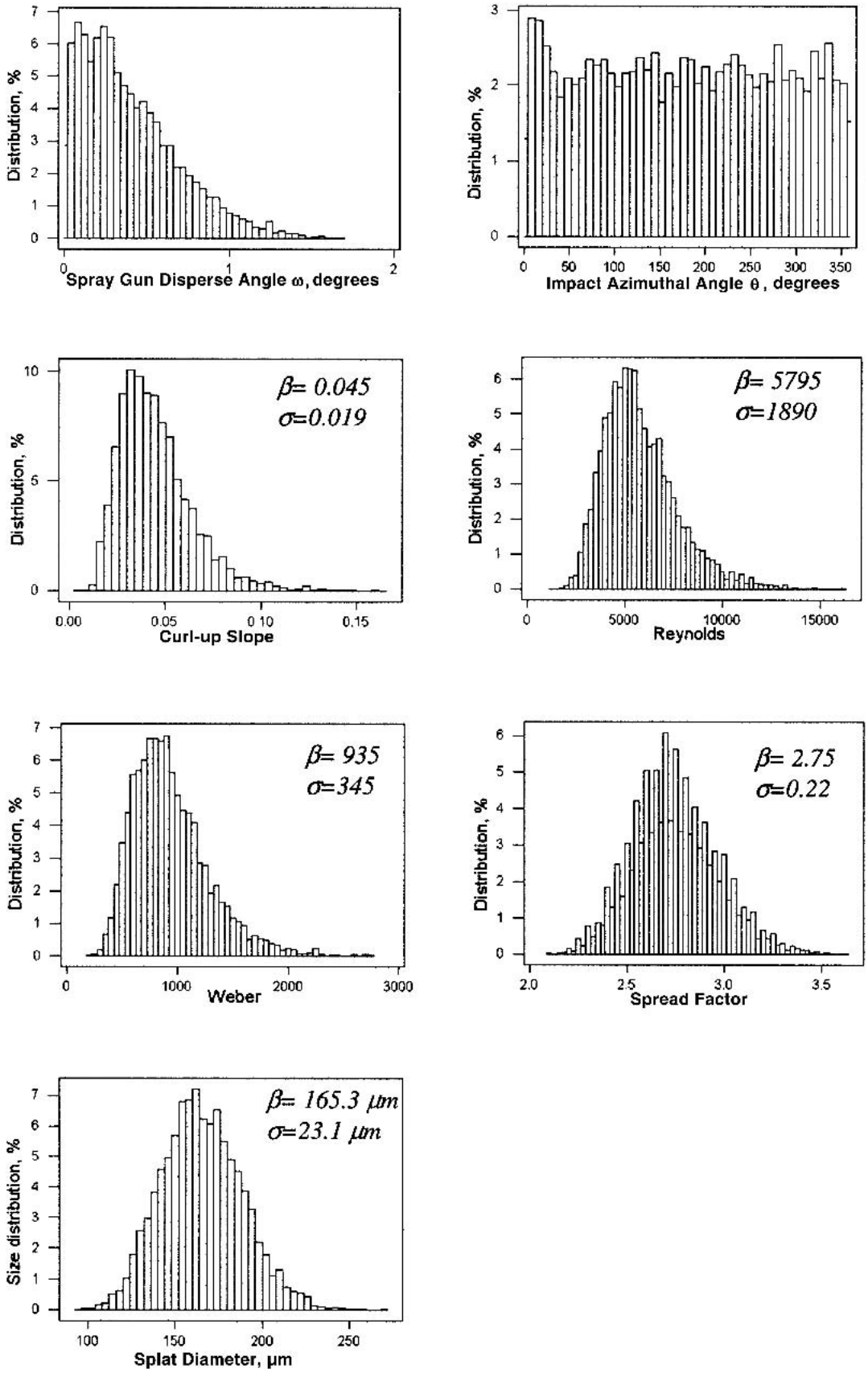

Fig. 12 Typical distributions of spray parameters generated by the model

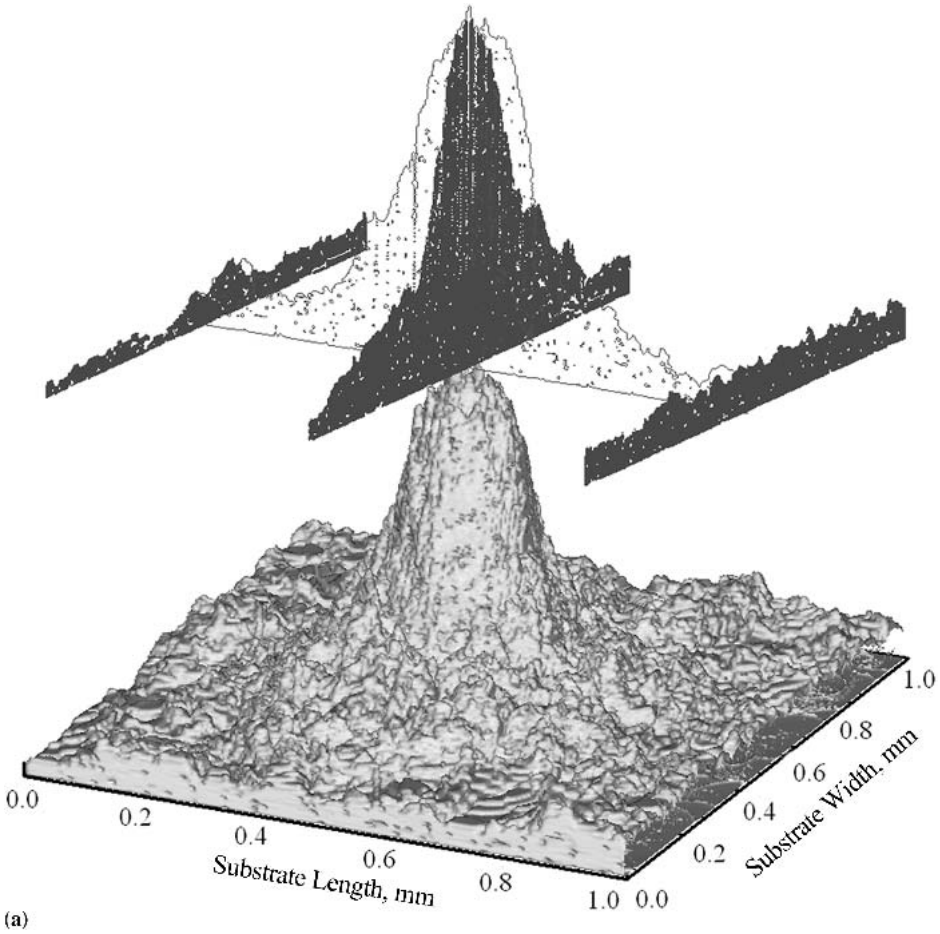

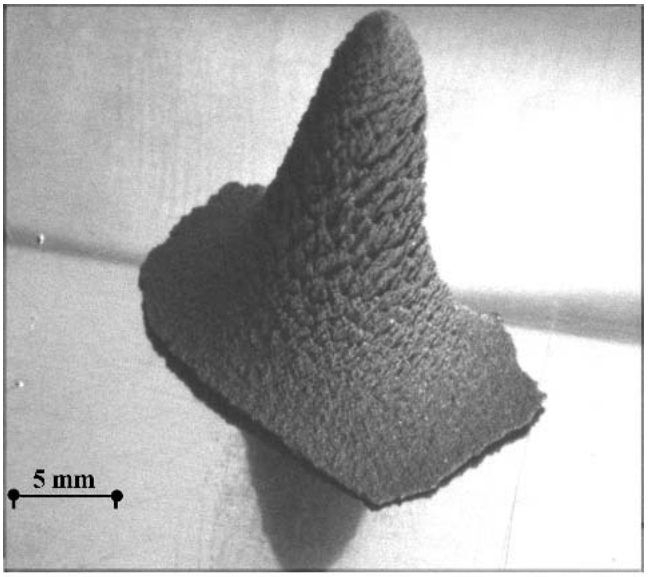

Fig. 13 Deposition of nickel particles in plasma spray by a spray gun held stationary over the substrate: **(a)** model and **(b)** micrograph

stationary. Though the size of the deposit is much larger than our simulation, the resemblance in shape is striking.

A three-dimension simulation of coating structure allows us to take cross sections through the coating at any desired plane. Figure 14 shows horizontal cross-section views through the deposit shown in Fig. 13(a), at heights of 3.4 μm (Fig. 14a), 64 μm (Fig. 14b), and 154 μm (Fig. 14c) above the substrate. The surfaces were taken to follow a contour corresponding to $f = 0.5$.

Figure 15 shows a simulated coating produced by a gun that moved with constant velocity. The substrate in this case was also 1 mm × 1 mm in size. The gun moved along its length (the x direction) at a speed of 1 m/s; once it reached the end it moved a distance of 12.8 μm in the y direction at a speed of 2 m/s, and then made another pass back along the length, repeating this motion for 0.072 s. All other parameters are those listed in Table 1. Movement of the gun produced a much more uniform coating than holding it stationary (Fig. 15).

Figure 16(a) shows a cross section through a coating made with a gun traveling with constant velocity 1 m/s, moving back and forth in the x direction only, on a substrate 1 mm × 1 mm in size. The total mass deposited was 5 mg, which took 0.039 s to spray. The cross section shown was made through the center-plane of the coating at y = 0.05 mm. We calculated the porosity p = 11.1%, average thickness $h_{c,m}$ = 0.422 mm, and average surface roughness R_a = 52 μm. The to-and-fro motion of the gun means that it spends twice the time at the center of the substrate that it does at its edges, so that the coating was thickest at the center.

A more uniform coating can be obtained by varying the gun velocity in a sinusoidal fashion, as given by Eq 19. This ensures that gun speed is lowest near the ends of the substrate (increasing the mass deposited) and maximum at its middle. Figure 16(b) shows the cross section through a coating deposited with a gun moving sinusoidally with a maximum velocity U_0 = 1 m/s. The total mass deposited and all other parameters were the same as that in Fig. 16(a). The porosity did not change significantly (p = 10.6%), but both average thickness ($h_{c,m}$ = 0.373 mm) and surface roughness (R_a = 41 μm) were reduced, reflecting the more even coating distribution. Note that during the spray process, in both cases, a portion of the propelled droplets from the spray gun landed out of the computational domain. For the case of the sinusoidal process, the gun spent more time at two edges of the substrate; therefore, the possibility that the droplets would fall outside the domain was greater. Therefore, the total coating material landing on the substrate was smaller compared with the constant speed case.

We ran simulations to evaluate the effect of varying process parameters such as particle speed and particle size on coating porosity, thickness, and roughness. In these simulations, all spraying parameters were the same as those in the previous case (on a 1 mm × 0.1 mm substrate) except that the gun speed was 0.1 m/s. Figure 17 shows the effect of varying particle speed on coating properties. The coating properties shown in the graphs were estimated along the plane passing through y = 0.05 mm, not for the whole 0.1 mm width of substrate. The standard deviation of the particle speed was chosen as 10% of the mean value, indicated by error bars in Fig. 17. Porosity decreased slightly, and coating thickness and roughness decreased by a larger amount when particle velocity increased. Splats flatten out more and become thinner at high impact velocity, making the coating thinner and smoother.

The effect of average particle size on coating properties is shown in Fig. 18. Average particle diameters were varied from 40-120 μm, with a standard deviation of 30%. Since the total coating mass sprayed was fixed, increasing particle size meant spraying fewer droplets. The coating porosity therefore decreased (Fig. 18a), because fewer voids were formed. Also, greater density of the coating meant that its thickness was much

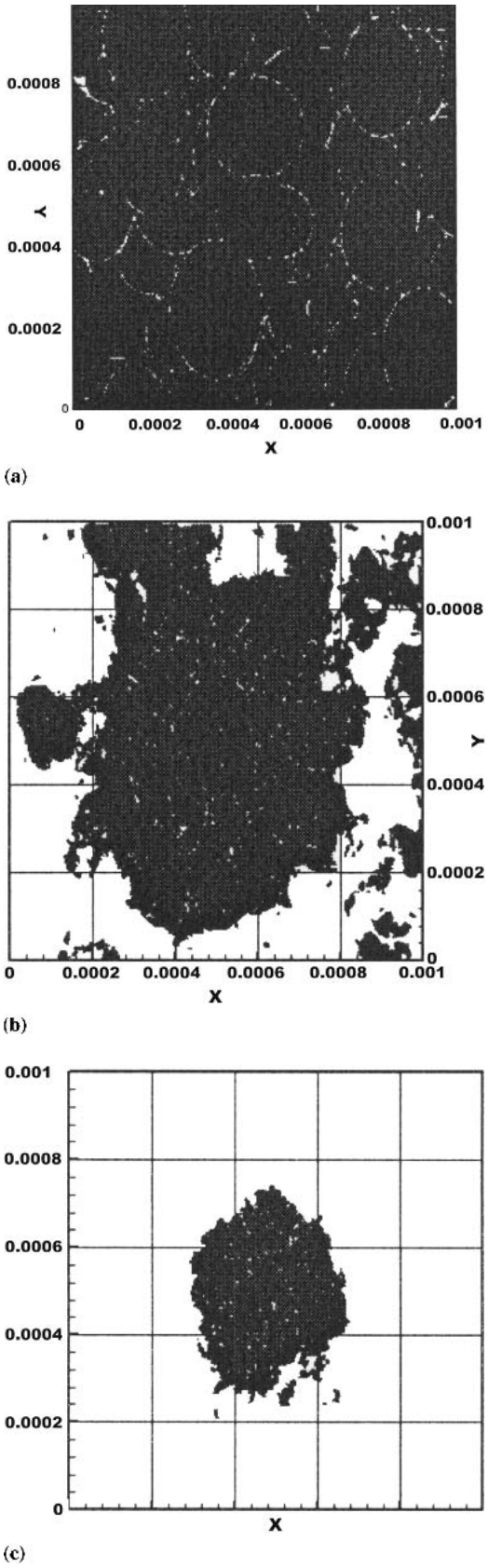

Fig. 14 Cross-sectional view of a coating structure produced by the model at elevation: **(a)** 3.4 μm, **(b)** 64 μm, and **(c)** 154 μm

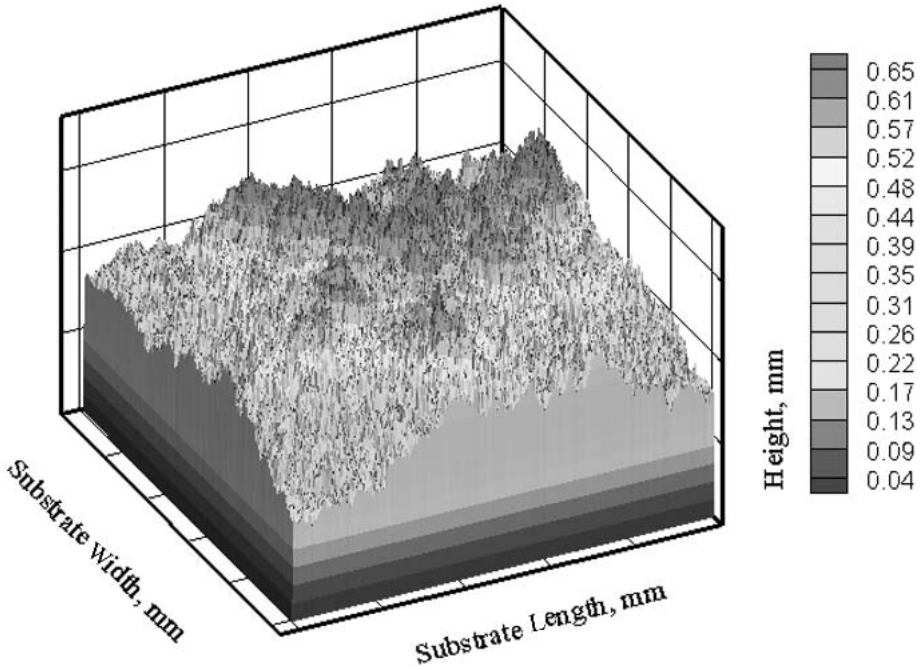

Fig. 15 Deposit formed by a spray gun moving with constant velocity over the substrate

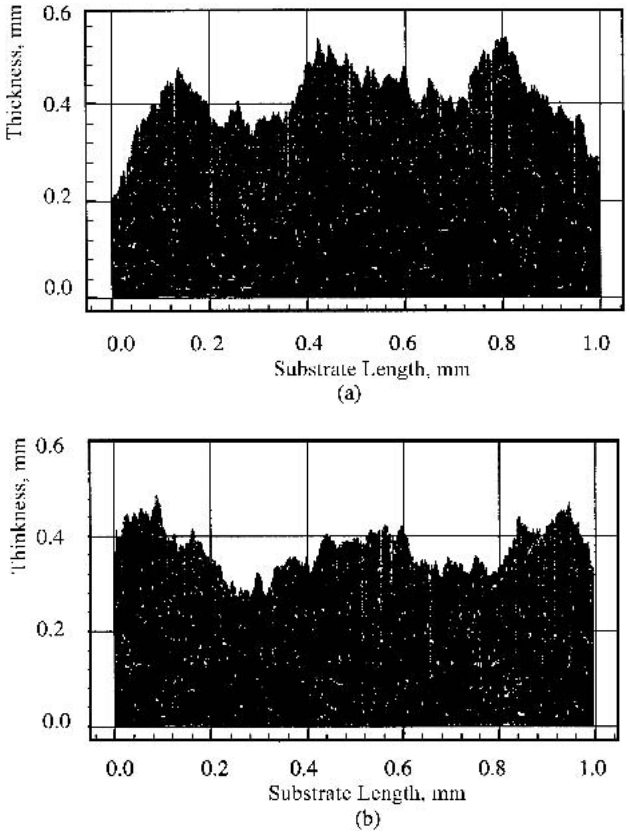

Fig. 16 Cross-sectional view of a coating made with **(a)** a gun with moving constant speed V_x = 1.0 m/s; the coating has the properties p = 11.1%, $h_{c,m}$ = 422.4 μm, R_a = 51.9 μm. **(b)** A gun moving with sinusoidally varying velocity with V_{nmax} = 1.0 m/s; the coating has the properties p = 10.6%, $h_{c,m}$ = 373.0 μm, R_a = 40.8 μm

less (Fig. 18b). Larger particles, however, produced greater surface roughness (Fig. 18c).

We simulated the deposition of particles using different gun travel speeds from 0.05-0.5 m/s, while keeping the powder feed rate constant at 0.126 g/s. Figure 19 shows that gun speed had little effect on porosity and coating thickness. Interestingly, surface roughness was minimized at a gun speed of 0.3 m/s (Fig. 19c). We have no experimental evidence of this phenomenon, but it requires further investigation.

4. Summary and Conclusion

A three-dimensional stochastic model based on the Monte Carlo method has been developed to simulate microstructure of thermal spray coatings as a function of process parameters. In the model, the coating was assumed to consist of splats deposited on each other, with voids between them leading to porosity. It was assumed that porosity is formed solely by the curl-up at the edges of individual splats due to thermal stresses. The model predicts the variation of coating porosity, thickness and roughness with particle impact velocity, and gun movement. Gun movement produced a much more uniform coating than holding it stationary. For the stationary gun, the surface of the deposit follows a Gaussian distribution, with its maximum thickness at the center of the deposit and decreasing with distance from this point. For a constant deposition mass, the numerical study of coating properties showed that when particle velocity increases, porosity decreases slightly, and coating thickness and roughness decrease by a larger amount. With the increasing particle average size, the coating porosity decreases. Larger particles, however, result in greater surface roughness. The predicted trends are in agreement with those observed experimentally.

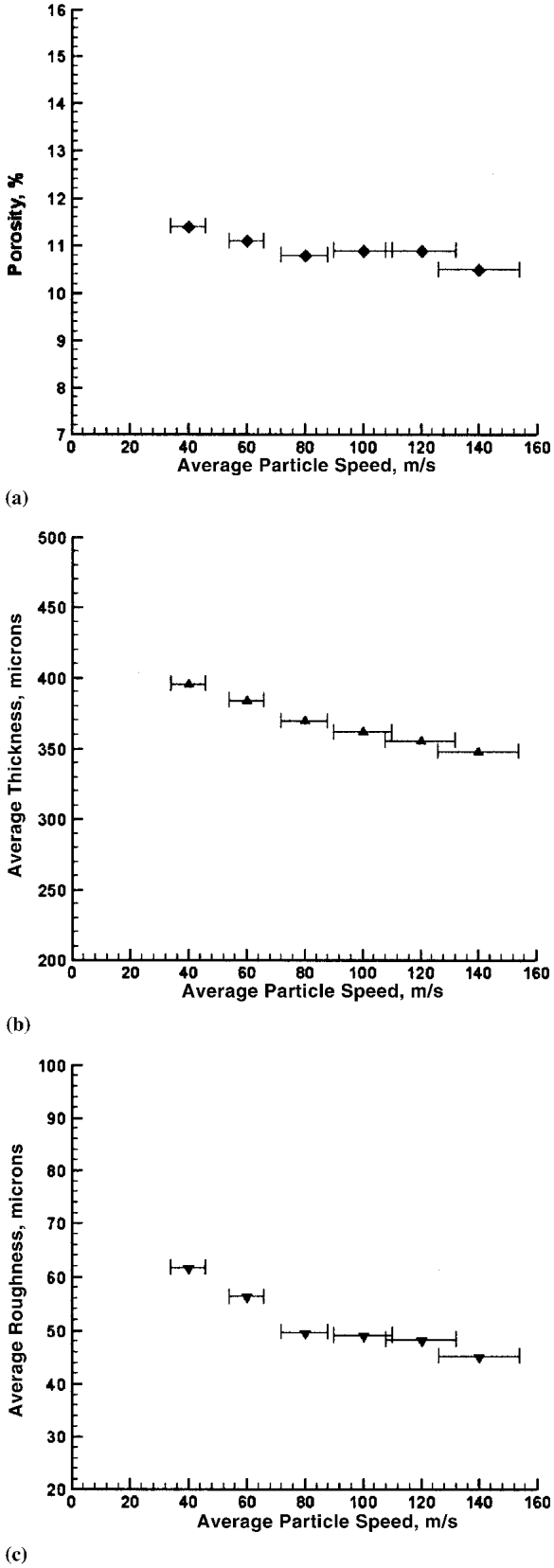

Fig. 17 Variations of **(a)** coating porosity, **(b)** average thickness, **(c)** average roughness with particle average speed. The substrate size is 1 mm.

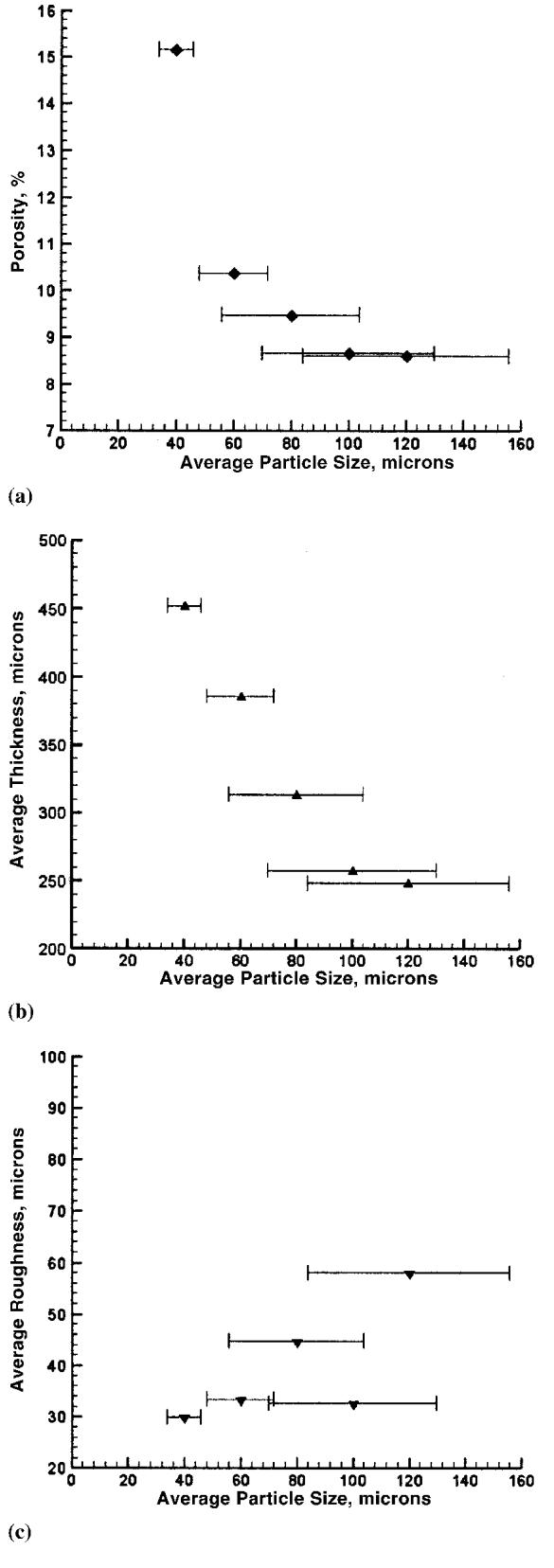

Fig. 18 Variations of **(a)** coating porosity, **(b)** average thickness, **(c)** average roughness with particle average diameter. The substrate size is 1 mm × 0. 1 mm, and the total coating mass deposited is 5 mg in all cases.

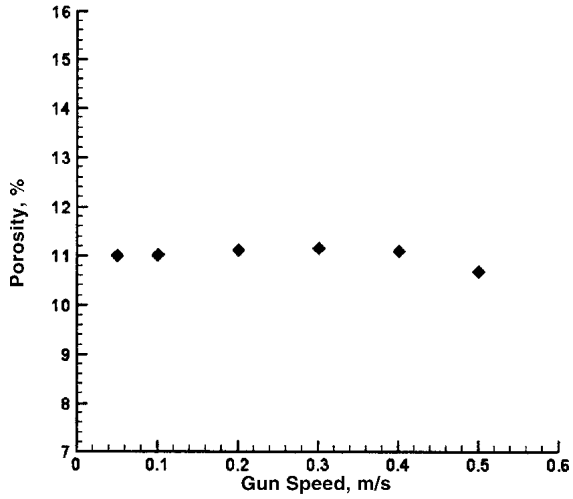

(a)

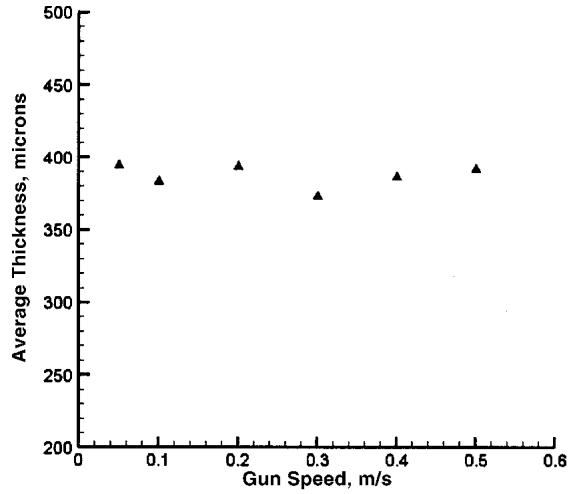

(b)

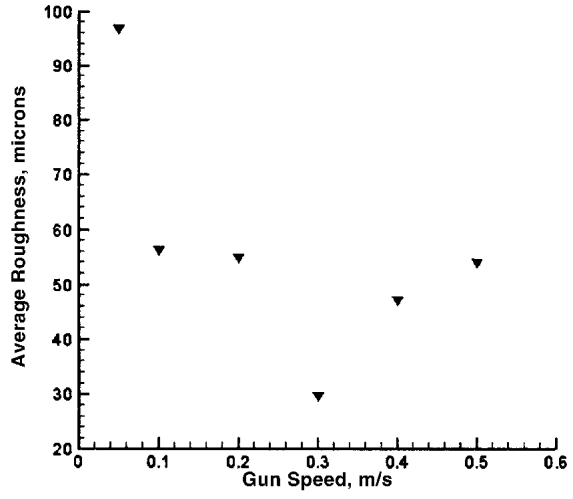

(c)

Fig. 19 Variations of **(a)** coating porosity, **(b)** average thickness, **(c)** average roughness with gun speed. The substrate size is 1 mm × 0.1 mm, and the total coating mass deposited is 5 mg in all cases.

Acknowledgments

This research was supported by the Natural Science and Engineering Research Council of Canada, Materials and Manufacturing Ontario, and member companies of the Center for Advanced Coating Technologies at the University of Toronto.

References

1. M. Vardelle, A. Vardelle, A.C. Leger, P. Fauchais, and D. Gobin: "Influence of Particle Parameters at Impact on Splat Formation and Solidification in Plasma Spraying Processes," *J. Therm. Spray Technol.*, 1995, *4*(1), pp. 50-58.
2. R. McPherson and B.V. Shafer: "Interlamellar Contact Within Plasma-Sprayed Coatings," *Thin Solid Films*, 1982, *97*, pp. 201-04.
3. R. McPherson: "A Review of Microstructure and Properties of Plasma Sprayed Ceramic Coatings," *Surf. Coat. Technol.*, 1989, *39/40*, pp. 173-81.
4. S. Safai and H. Herman: "Microstructure Investigation of Plasma-Sprayed Aluminum Coatings," *Thin Solid Films*, 1977, *45*, pp. 295-307.
5. O. Knotek and R. Elsing: "Monte Carlo Simulation of the Lamellar Structure of Thermally Sprayed Coatings," *Surf. Coat. Technol.*, 1987, *32*, pp. 261-71.
6. S. Cirolini, H. Harding, and G. Jacucci: "Computer Simulation of Plasma-Sprayed Coatings Deposition Model," *Surf. Coat. Technol.*, 1991, *48,* pp. 137-45.
7. S. Cirolini, M. Marchese, G. Jacucci, J.H. Harding, and P.A. Mulheran: "Modeling the Microstructure of Thermal Barrier Coatings," *Mater. Design Technol., ASME*, 1994, *162,* pp. 189-98.
8. M.P. Kanouff, R.A. Nieser, and T.J. Roemer: "Surface Roughness of Thermal Spray Coating Made With Off-Normal Spray Angle," *J. Therm. Spray Technol.*, 1998, *7*(2), pp. 219-28.
9. A. Hansbo and P. Nylen: "Models for the Simulation of Spray Deposition and Robot Motion Optimization in Thermal Spraying of Rotating Objects," *Surf. Coat. Technol.*, 1999, *122*(2-3), pp. 191-201.
10. J. Madejski: "Solidification of Droplets on a Cold Surface," *Int. J. Heat and Mass Transfer*, 1976, *19*, pp. 1009-13.
11. Z. Zhao, D. Poulikakos, and J. Fukai: "Heat Transfer and Fluid Dynamics During the Collision of a Liquid Droplet on a Substrate-I. Modeling," *Int. J. Heat and Mass Transfer*, 1996, *39*(13), pp. 2771-89.
12. Z. Zhao, D. Poulikakos, and J. Fukai: "Heat Transfer and Fluid Dynamics During the Collision of a Liquid Droplet on a Substrate-II. Experiments," *Int. J. Heat and Mass Transfer*, 1996, *39*(13), pp. 2791-802.
13. M. Pasandideh-Fard, R. Bhola, S. Chandra, and J. Mostaghimi: "Deposition of Tin Droplets on a Steel Plate: Simulations and Experiments," *Int. J. Heat and Mass Transfer*, 1998, *41*(19), pp. 2929-45.
14. M. Bussmann, J. Mostaghimi, and S. Chandra: "On a Three-Dimensional Volume Tracking Model of Droplet Impact," *Phys. Fluids*, 1999, *11*(6), pp. 1406-17.
15. M. Pasandideh-Fard, J. Mostaghimi, and S. Chandra: "On a Three-Dimensional Model of Free Surface Flows With Heat Transfer and Solidification" in *Proc. 3rd ASME/JSME Joint Fluids Engineering Conf.*, San Francisco, CA, 1999, FEDSM99-7112.
16. R. Bhola and S. Chandra: "Parameters Controlling Solidification of Molten Wax Droplets Falling on a Solid Surface," *J. Mater. Sci.*, 1999, *34*(19), pp. 4883-94.
17. C. Moreau, P. Cielo, and M. Lamonta: "Flattening and Solidification of Thermal Sprayed Particles" in *Proc. International Thermal Spray Conf. & Exposition*, ASM International, Orlando, FL, 1992, pp. 761-66.
18. D. Attinger, Z. Zhao, and D. Poulikakos: "An Experimental Study of Molten Microdroplet Surface Deposition and Solidification: Transient Behavior and Wetting Angle Dynamics, *J. Heat Transfer*, *122*(3), 2000, pp. 544-56.
19. S. Aziz and S. Chandra: "Impact, Recoil and Splashing of Molten Metal Droplets," *Int. J. Heat and Mass Transfer,* 2000, *43*(16), pp. 2841-57.
20. M. Fukumoto and Y. Huang: "Flattening Mechanism in Thermal Sprayed Nickel Particle Impinging on Flat Substrate Surface," *J. Therm. Spray Technol.*, 1999, *8*(3), pp. 427-32.
21. J.F. Bisson, B. Gauthier, and C. Moreau: "Effect of Plasma Fluctuations

on In-Flight Particle Parameters" in *Thermal Spray 2001: New Surfaces for a New Millennium,* C.C. Berndt, K.A. Khor, and E.F. Lugscheider, ed., ASM International, Singapore, 2001, pp. 715-21.
22. L. Pouliot, J. Blain, F. Nadeau, M. Lamontagne, J.F. Bisson, and C. Moreau: "Optimization and Monitoring of Spray Parameters by a CCD Camera Based Imaging Thermal Spray Monitor" in *Thermal Spray 2001: New Surfaces for a New Millennium,* C.C. Berndt, K.A. Khor, and E.F. Lugscheider, ed., ASM International, Singapore, 2001, pp. 723-26.
23. C.T.Crowe, M. Sommerfeld, and Y. Tsuji: *Multiphase Flows With Droplets and Particles*, CRC Press, Boca Raton, FL, 1998.
24. G.S. Fishman: *Monte Carlo: Concepts, Algorithms, and Applications*, Springer-Verlag, New York, NY, 1996.
25. S. Shakeri: "Effect of Substrate Properties on Molten Metal Droplet Impact", M.A.Sc. Thesis, University of Toronto, Toronto, Ontario, Canada, 2001.
26. R. Ghafouri-Azar, S. Shakeri, S. Chandra, and J. Mostaghimi: "Numerical Simulation of Offset Deposition for Sequential Tin Droplets" in *Proc. International Thermal Spray Conf. & Exposition 2002*, Essen, Germany, 4-6 Mar, 2002, pp. 951-59.
27. W.D. Cai and E.J. Lavernia: "Modeling of Porosity During Spray Forming," *Mater. Sci. Eng. A*, 226-228, 1997, pp. 8-12.
28. H. Fukanuma: "A Porosity Formation and Flattening Model of an Impinging Molten Particle in Thermal Spray Coatings," *J. Therm. Spray Technol.*, 1994, *3*(1), pp. 33-44.